1-1-2022

Towards a digital twin for characterising natural source zone depletion: A feasibility study based on the Bemidji site

Kaveh Sookhak Lari
Edith Cowan University, kaveh.sookhaklari@unisa.edu.au

Greg B. Davis

John L. Rayner

10.1016/j.watres.2021.117853
Lari, K. S., Davis, G. B., & Rayner, J. L. (2022). Towards a digital twin for characterising natural source zone depletion: A feasibility study based on the Bemidji site. Water Research, 208, article 117853. https://doi.org/10.1016/j.watres.2021.117853

Water Research 208 (2022) 117853

Contents lists available at ScienceDirect

Water Research

journal homepage: www.elsevier.com/locate/watres

Towards a digital twin for characterising natural source zone depletion: A feasibility study based on the Bemidji site

Kaveh Sookhak Lari [a,b,*], Greg B. Davis [a,c], John L. Rayner [a]

[a] CSIRO Land and Water, Private Bag No. 5, Wembley, WA 6913, Australia
[b] School of Engineering, Edith Cowan University, 270 Joondalup Drive, Joondalup, WA 6027, Australia
[c] School of Earth Sciences, The University of Western Australia, 35 Stirling Highway, Crawley,WA 6009, Australia

ARTICLE INFO

Keywords:
NSZD
Multi-phase
Multi-component
Multi-microbe
Non-isothermal
Digital twin

ABSTRACT

Natural source zone depletion (NSZD) of light non-aqueous phase liquids (LNAPLs) may be a valid long-term management option at petroleum impacted sites. However, its future long-term reliability needs to be established. NSZD includes partitioning, biotic and abiotic degradation of LNAPL components plus multiphase fluid dynamics in the subsurface. Over time, LNAPL components are depleted and those partitioning to various phases change, as do those available for biodegradation. To accommodate these processes and predict trends and NSZD over decades to centuries, for the first time, we incorporated a multi-phase multi-component multi-microbe non-isothermal approach to representatively simulate NSZD at field scale. To validate the approach we successfully mimic data from the LNAPL release at the Bemidji site. We simulate the entire depth of saturated and unsaturated zones over the 27 years of post-release measurements. The study progresses the idea of creating a generic digital twin of NSZD processes and future trends. Outcomes show the feasibility and affordability of such detailed computational approaches to improve decision-making for site management and restoration strategies. The study provided a basis to progress a computational digital twin for complex subsurface systems.

1. Introduction

Anthropogenic releases of petroleum hydrocarbons, some accidental and some not, can be harmful to the environment. Fixed and storage facilities, and pipelines, make up the bulk of these releases (Etkin, 2009a, 2001, 2009b; Sookhak Lari et al., 2021), for example, contributing over 34,000 m^3 per year to land and groundwater resources in the United States of America alone (Etkin, 2009a, 2009b). Accidental oil spills are still a global challenge and it is estimated that 74% occurs at refineries, oil terminals or storage tanks with a proportionality of 47% in North America, 29% Asia, 16% Europe, 4% Africa and 4% South America (Chang and Lin, 2006; Chilvers et al., 2021; Fingas, 2012; Khan and Abbasi, 1999).

Releases of such light non-aqueous phase liquid (LNAPL) petroleum products expose the environment to thousands of chemicals some with significant health risk profiles. Upon release at ground surface, LNAPL plumes travel downwards through a vadose zone leaving residual LNAPL mass in the soil profile as it moves towards groundwater. Spreading of the LNAPL plume over the capillary fringe augments interphase mass transfer. The residual LNAPL mass as well as the main body of the plume can remain as a source of contamination of subsurface gaseous (Davis et al., 2021) and aqueous phases (Lekmine et al., 2017) for decades (Garg et al., 2017; Sookhak Lari et al., 2016a; Sookhak Lari et al., 2019a; Sookhak Lari et al., 2016b; Sookhak Lari et al., 2020).

Active remediation approaches target LNAPL recovery in different phases or thermal, biological and chemical destruction of the target chemicals. However, the performance of restoration technologies is a complex function of the release event, the LNAPL itself, the subsurface stratigraphy, and the configuration of the applied remedial technology (Sookhak Lari et al., 2018a; Sookhak Lari et al., 2018b; Sookhak Lari et al., 2020). Several studies have shown that even after remediation and recovery approaches reach an endpoint of limited additional LNAPL mass removal, still a significant portion of the LNAPL can continue to reside in the form of residual or entrapped mass (Lenhard et al., 2018; Sookhak Lari et al., 2020). Beyond and concurrent with active remedial efforts, LNAPL mass depletion occurs via partitioning and biodegradation of LNAPL components – and recently this has been referred to as natural source zone depletion (NSZD).

NSZD of LNAPL includes biodegradation and partitioning of LNAPL compounds in different phases and has received significant attention

* Corresponding author at: CSIRO Land and Water, Private Bag No. 5, Wembley, WA 6913, Australia.
E-mail address: kaveh.sookhaklari@csiro.au (K. Sookhak Lari).

https://doi.org/10.1016/j.watres.2021.117853
Received 7 September 2021; Received in revised form 5 November 2021; Accepted 6 November 2021
Available online 10 November 2021

over the last decade (Garg et al., 2017; Sookhak Lari et al., 2019a). NSZD starts immediately after the release and consists of a dynamic sequence of complex biological processes. In some circumstances biodegradation processes may shift to be dominated by methanogenesis (Garg et al., 2017). Along with transport of volatile organic gases through the vadose zone, methanogenesis (and subsequence methane and carbon dioxide formation mainly adjacent to the LNAPL plume, known as direct outgassing) can play a primary role in LNAPL mass loss (Garg et al., 2017). The rate of NSZD through methanogenesis can be considerable in comparison to the rate of LNAPL recovery close to the endpoint of active LNAPL recovery from wells (e.g. 0.65 to 2.6 L/m^2/year equal to 700 to 2800 gallons/acre/year) (Garg et al., 2017; Sookhak Lari et al., 2018b; Sookhak Lari et al., 2020).

Regulatory decisions on whether the residual LNAPL mass may be left in the subsurface is a function of the risk profile of the remaining LNAPL and the rate of NSZD (Bekins et al., 2005). The rate of NSZD may vary over time and is a complex function of the LNAPL composition and saturation, and the presence of electron acceptors and nutrients (Freitas et al., 2011a,b, Molson et al., 2002a,b). NSZD rates may be estimated via a range of measurements and approaches (e.g., CRC-CARE 2018), including, for example surface flux of carbon dioxide, temperature increases, and consumed and produced major gases (Davis et al., 2013; Karimi Askarani and Sale, 2020; Knight and Davis, 2013; Kulkarni et al., 2020; Rayner et al., 2020; Smith et al., 2021; Verginelli and Baciocchi, 2021). However, predicting future transitions in NSZD rates and LNAPL risks, along with links to other remedial actions requires representative modeling encompassing all of the key features of LNAPL dynamics and associated NSZD mass removal processes. A critical review paper on the state-of-the-art modeling approaches and studies on NSZD has recently been published (Sookhak Lari et al., 2019a).

We present here for the first time a simulation platform to progress towards a digital twin of all the relevant NSZD partitioning and biodegradation processes linked to LNAPL multiphase processes occurring in the subsurface. We evaluate its performance and reliability against published data and outcomes associated with the well characterised Bemidji site where crude oil was released into the subsurface over 40 years ago (Baedecker et al., 2018; Essaid et al., 2011). We apply a multi-phase multi-component multi-microbe and non-isothermal modeling framework for the Bemidji site (the north pool); and characterise NSZD processes over the entire depth of the formation (saturated and unsaturated). Our primary aim is to assess the feasibility of using such a complex computational modeling framework to study real cases and establish confidence in long term NSZD sustainability.

2. NSZD digital twin modeling platform and approach

A comprehensive review of possible modeling approaches was undertaken by Sookhak Lari et al. (2019a). To date, the most-applied models include one-dimensional gaseous phase transport in the vadose zone (Baedecker et al., 1993; Sihota et al., 2011) and two-dimensional models focusing either on the saturated or unsaturated zone (Amos and Mayer, 2006; Mayer et al., 2002; Molins et al., 2010; Ng et al., 2015; Ng et al., 2014). The first includes two phase reactive transport of aqueous and gaseous phases in the vadose zone and the second includes reactive solutes transport in the groundwater. Following a recent review paper on modeling NSZD (Sookhak Lari et al., 2019a) and a more recent literature review, the authors are still not aware of a multi-phase (NAPL, soil gas and water), multi component (NAPL components, soil gases and solutes), multi-microbe (aerobic, anaerobic and methanogenesis) and non-isothermal modeling platform being established or applied for a real contaminated site.

Digital twin refers to a comprehensive (physical and functional) description of a system, which includes all the most-useful information, over the lifecycle phases. It is an emerging representation of cyber-physical systems and has attracted increasing attention very recently. Through this concept, a digital representation of the system under study is developed. The level of the complexity applied in the digital twin is a function of the computational infrastructure and collected data. Nevertheless, this concept opens the way to real-time monitoring and synchronization of real-world phenomena with virtual counterparts (Boschert and Rosen, 2016; Grieves and Vickers, 2017; Liu et al., 2021; VanDerHorn and Mahadevan, 2021). The concept is most-widely applied in manufacturing or controlled engineering systems, but despite this it has become a subject of interest in other fields such as environmental engineering (Conejos Fuertes et al., 2020). Its application to study NSZD is not yet reported (Liu et al., 2021).

Recently more than 30 codes were compared with respect to their capabilities in addressing and mimicking major NSZD processes (Sookhak Lari et al., 2019a). Among them, TMVOCBio showed the greatest potential for developing digital twins for LNAPL-contaminated sites undergoing NSZD. The most-recent parallel-processing version of the code has been released with TOUGH3 (Jung et al., 2017).

Major features of TMVOCBio, now released as a part of TOUGH3 group of codes, include combining the multi-phase multi-component non-isothermal modeling capabilities in TMVOC with a general modified form of the Monod kinetic rate equation to simulate biodegradation reactions. The code can account for various limiting factors such as limitation by substrate, electron acceptor, or nutrients. The biodegradation may be simulated as a multiple Monod kinetic rate equation, or a minimum Monod model. Biomass growth inhibition, toxicity effects and competitive and non-competitive inhibition effects are included as limiting factors. The temperature and moisture dependence of biodegradation processes are also considered (Battistelli, 2004; Jung and Battistelli, 2017).

3. The model and governing equations

TMVOCBio is a finite volume numerical simulator (based on TOUGH3) for multi-phase multi-component multi-microbe transport phenomena at a Darcy scale. The substrate utilisation rate (r_s) and biomass growth/decay in the code are governed by (Barry et al., 2002; Battistelli, 2004):

$$\mathrm{r_s} = -\mu_{\max}\frac{\mathrm{X}}{\mathrm{I}}\left(\frac{\mathrm{S}}{\mathrm{K_s}+\mathrm{S}}\right)\left(\frac{\mathrm{E}}{\mathrm{K_E}+\mathrm{E}}\right) \tag{1}$$

$$\frac{\mathrm{dX}}{\mathrm{dt}} = -\mathrm{Yr_s} - \mathrm{bX} \tag{2}$$

where X, E and S are the biomass, electron acceptor and substrate concentrations respectively [M/L^3], K_s and K_E are the half-saturations of the substrate and electron acceptor [M/L^3], $\mathrm{I} = -\left(\frac{\mathrm{S}+\mathrm{K_{NC}}}{\mathrm{K_{NC}}}\right)$ is the non-competitive inhibition factor, $\mathrm{K_{NC}}$ is the non-competitive inhibition coefficient, $\mu_{\max}$ is the maximum specific growth rate [T^{-1}], Y is the biomass yield coefficient and b [T^{-1}] is the first-order decay coefficient (Blanc et al., 1996).

Multi-phase flow models can simulate the simultaneous transport of aqueous, gaseous and LNAPL phases. The mass transport equation is (Miller et al., 2013; Pruess and Battistelli, 2002)

$$\frac{\partial C^i}{\partial t} + \nabla.\left[\sum_{\beta=1}^{N_p}\left(C^i_\beta\, v_\beta - D\,\nabla C^i_\beta\right)\right] = r^i \tag{3}$$

where i and β refer to the component number k and phase β respectively (with N_p as the total number of phases), D is the (effective) diffusion coefficient [MT^{-1}] and r is the sink/source term. The velocity v is calculated through the Darcy law equation:

$$v_\beta = -k\frac{k_{r\beta}}{\mu_\beta}\left(\nabla P_\beta - \rho_\beta \boldsymbol{g}\right) \tag{4}$$

with constitutive relationships to relate relative permeability of each

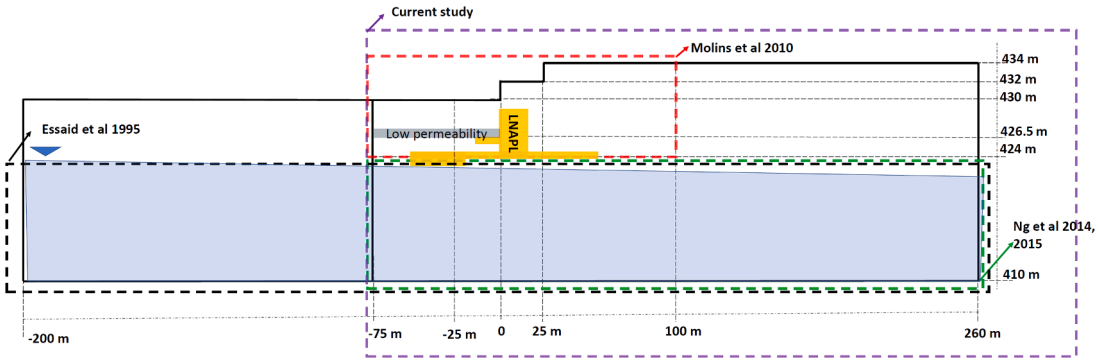

Fig. 1. Conceptual site model and position of the current modeling study with respect to previous studies at the site.

phase, pressure (P, including capillary) and the phase saturation (Lenhard and Parker, 1990). Here, k and $k_{r\beta}$ are the absolute and relative permeability to phase β ([L^2] and [-] respectively), ρ and μ are the density [ML^{-3}] and viscosity of phase β [$ML^{-1}T^{-1}$] and g is the gravity acceleration vector [LT^{-2}]. The constitutive relationship (van Genuchten equation) between saturation and head ($h = P/\rho g$) is

$$\frac{S_j^{ij} - S_m}{1 - S_m} = \left[1 + (\alpha_{ij} h)^n\right]^{-m}, i, j = G, Aq, N, i \neq j \quad (5)$$

where S_j^{ij} represents the effective wetting phase fluid saturation, n is a constant, $m = 1/n - 1$ and S_m is the irreducible saturation (of the wetting phase).

The three-phase fluid flow requires the relative permeability to be a function of phase saturation. We apply the van Genuchten-Muallem equation in the model for the relative permeabilities to gas (G), aqueous (Aq) and LNAPL (N) phases (Jung and Battistelli, 2017; Parker and Lenhard, 1987):

$$k_{rG} = \sqrt{\overline{S_G}}\left(1 - \overline{S}_L^{1/m}\right)^{2m} \quad (6)$$

$$k_{rAq} = \sqrt{\overline{S_{Aq}}}\left(1 - \left(1 - \overline{S}_{Aq}^{1/m}\right)^{m}\right)^{2} \quad (7)$$

$$k_{rN} = \sqrt{\overline{S_L} - \overline{S_N}}\left(\left(1 - \overline{S}_{Aq}^{1/m}\right)^{m} - \left(1 - \overline{S_L}^{1/m}\right)^{m}\right)^{2} \quad (8)$$

where the saturations are in their effective form, with L representing the total liquid (Parker and Lenhard, 1987). The model includes partitioning of compounds in three phases, by considering equilibrium conditions (Raoult's and Henry's law) (Jung et al., 2017; Lekmine et al., 2017; Sookhak Lari et al., 2015; Sookhak Lari et al., 2017). Here the phase mole fraction, vapour pressure and solubility of the compounds drive their concentration in other phases. Information for the LNAPL compounds may be found in the Supplementary Materials (INFILE) (Pruess and Battistelli, 2002).

Values for the biodegradation variables are reported in Table A1. Also the reader is referred to the attached model files (mainly INFILE) and the code manual (Jung and Battistelli, 2017) for complementary details. Geophysical properties are discussed in Section 4.1. The multi-component properties of the LNAPL are discussed in Section 4.2. Details of the microbial processes are presented in Section 4.3. The modeling domain and features are discussed first.

4. Features of the Bemidji site

A crude oil LNAPL accidental release occurred in August 1979 near Bemidji Minnesota (USA). It was estimated that 1.7×10^6 L was released and that remediation removed about 1.2×10^6 L. Later in 2000s, an additional 1.4×10^5 L were also recovered (Essaid et al., 2011). The remaining mass formed three separate LNAPL (oil) bodies, as residual mass in the vadose zone and as plumes close to the capillary fringe.

The north pool of the LNAPL has been comprehensively studied (Baedecker et al., 1993; Bekins et al., 2001; Bekins et al., 2005; Cozzarelli et al., 2001). Several studies on the site include modeling efforts to characterise the magnitude of NSZD at the north pool. One-dimensional modeling on the effect of oil biodegradation are numerous (Baedecker et al., 1993; Sihota et al., 2011). Two-dimensional two-phase studies of the vadose zone mostly used MIN3P and Min3P-Dusty to simulate reactive gas transport in the unsaturated zone (Amos and Mayer, 2006; Mayer et al., 2002; Molins et al., 2010). Comprehensive studies on reactive transport in the saturated zone are also available (Ng et al., 2015; Ng et al., 2014). However, no multi-phase multi-component modeling framework across the entire depth interval of the vadose zone and groundwater has been applied.

4.1. Site stratigraphy and soil characteristics

The lithology of the site is reported in numerous documents (Dillard et al., 1997; Essaid et al., 2003). A more recent publication also provides further details of the site measurements studies over a 25-year period (Essaid et al., 2011). Studies suggest that the average horizontal intrinsic permeability at the north pool is 10^{-12} m^2, with the vertical permeability one order of magnitude lower. As schematically depicted in Fig. 1, there is also a low permeability lens with a permeability of 10^{-13} m^2 (Essaid et al., 2003; Molins et al., 2010; Ng et al., 2015). It is suggested that the gas bubble formation at the vicinity of the LNAPL plume diminishes the permeability (Amos and Mayer, 2006; Essaid et al., 2003; Mayer et al., 2002). This phenomenon has also been observed during active remediation (Krol et al., 2011). In contrast with modeling packages like UTCHEM, TMVOCBio does not directly consider the effect of discrete gas bubbles on reducing the permeability (Sookhak Lari et al., 2019a). Following preliminary simulations, and accounting for these effects the permeabilities here were taken to be one order of magnitude lower than more permeable portions of the formation. The reported porosity is also 0.38 (Essaid et al., 2003).

Ranges for the soil characteristic curve (van Genuchten) parameters have been variably reported for the site. We use the values reported in Molins et al. (2010), $\alpha = 3.0$ m^{-1} and $n = 2.0$. The average hydraulic gradient of the water table is reported to be 0.0035 m/m, with the water table elevation of 424 m (above the sea level) on the left boundary (Essaid et al., 2003). Thermal heat conductivity of the site (from the water table to the surface) ranges from 0.4 to 2.0 W m^{-1} °C^{-1} (Jones et al., 2014; Warren and Bekins, 2015). We consider a heat conductivity of 0.8 W m^{-1} °C^{-1} to give more weight to the LNAPL zone (where the heat is generated). We consider a background uniform temperature of 9 °C (Warren and Bekins, 2015).

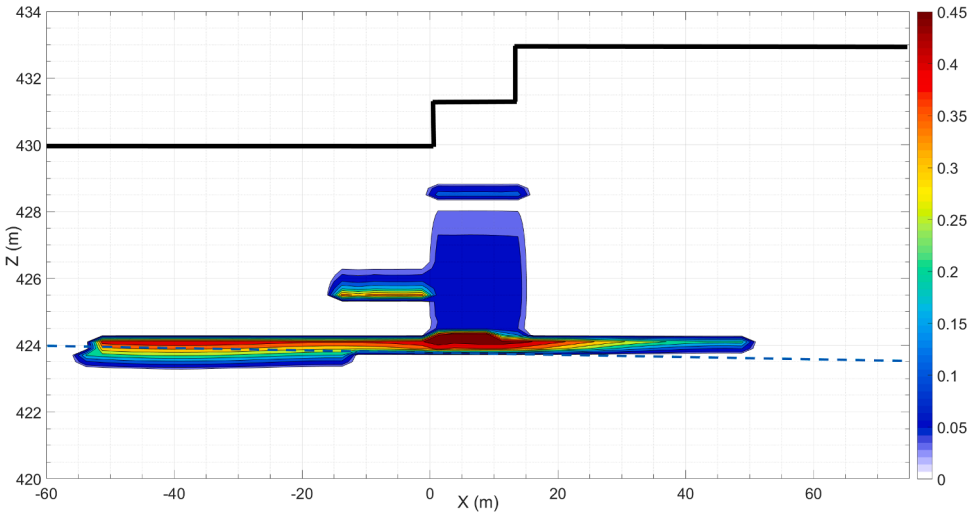

Fig. 2. Depth section of the estimated initial LNAPL plume saturation distribution. The upper black line is representative of the ground surface. The colorbar shows the LNAPL saturation [-].

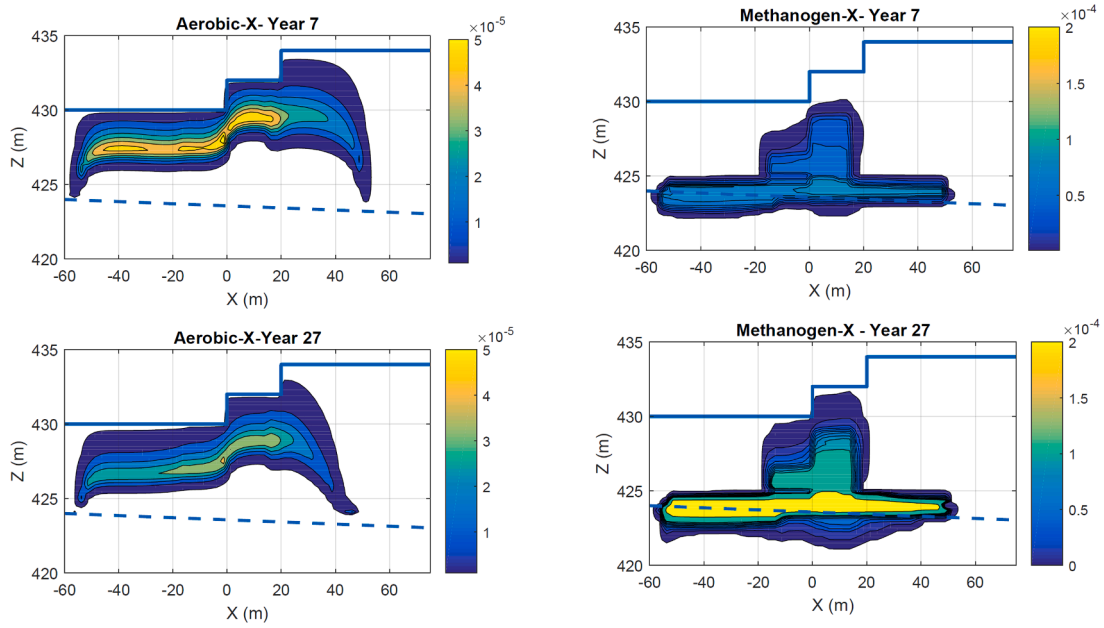

Fig. 3. Depth section of the aerobic (left) and methanogenic (right) microbial colonies (kg biomass / kg aqueous phase) after 7 and 27 years of simulation. The upper blue solid line is the ground surface, and the blue dashed line is the water table.

4.2. Multi-phase LNAPL compositions

It is estimated that 40% of the initial LNAPL released resided in the unsaturated zone (Ng et al., 2015). Data on the spatial distribution of the LNAPL saturation in the vadose zone and the saturated zone (Baedecker et al., 1993; Molins et al., 2010; Ng et al., 2015; Ng et al., 2014) were averaged to reproduce the initial LNAPL plume, as depicted in Fig. 2.

Following the approach in Ng et al. (2014), the crude oil was assumed to be composed of BEX (benzene, ethylbenzene and xylene, represented by C_6H_6), toluene (C_7H_8), precursors of non-volatile dissolved organic compounds (preNVDOC, $C_{19}H_{24}O_6$), short-chain ($C_{11}H_{25}$) and long-chain alkanes ($C_{15}H_{32}$) and residual NAPL (with a molar weight of 341 g/mole). The reported molar fractions of these are 0.35%, 1.0%, 40%, 7.4%, 10.0% and 40.0% respectively. Major mineral electron acceptors are Fe^{3+} and Mn^{4+} salts. In order to embed such minerals reduction reactions into TMVOCBio (which is not directly possible), we assume these are quasi-LNAPL compounds (with a saturation less than 0.1%) across the entire formation, with a bioavailable mass of 0.0288 and 0.001 mol per litre volume of the aquifer respectively (Ng et al., 2015). We also consider four major gases, nitrogen, oxygen, carbon dioxide and methane to be present or to be evolving in the subsurface.

4.3. Biodegradation processes and microbial dynamics

Monod-based biodegradation processes and growth and decay of counterpart microbial colonies, including non-competitive inhibitors, are considered, including aerobic degradation, Fe(III) and Mn(IV) reduction, and methanogenesis. Overall, 20 processes were included as part of the TMVOCBio simulation platform: (i) aerobic degradation, Fe and Mn reduction and methanogenesis of BEX, toluene and short-chain alkanes, (ii) aerobic degradation and Fe reduction of long chain alkanes, (iii) aerobic degradation of methane, (iv) methanogenesis of long-chain alkanes and (v) aerobic degradation, Fe reduction and methanogenesis

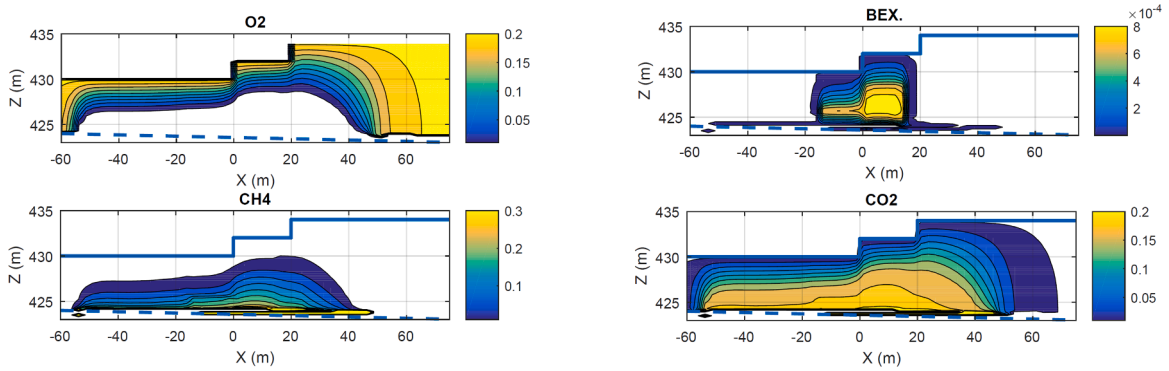

Fig. 4. Depth section of the mole fractions of oxygen (O_2), methane (CH_4), carbon dioxide (CO_2) and BEX in the gaseous phase at 27 years of simulation. The upper blue solid line is the ground surface, and the blue dashed line is the water table.

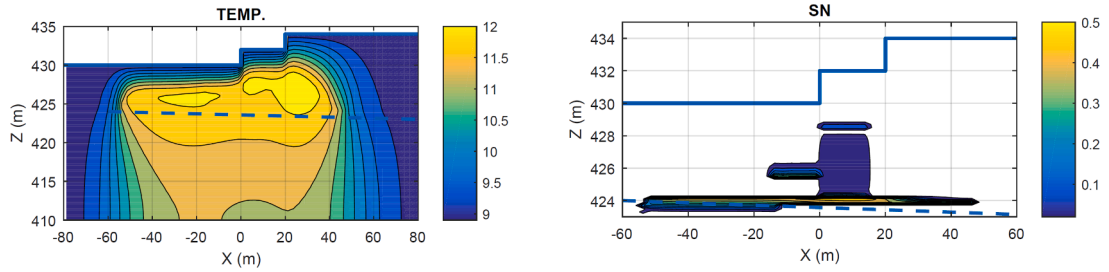

Fig. 5. Depth section for temperature (TEMP – left panel) and LNAPL saturation (SN – right panel) at the end of simulation. The upper blue solid line is the ground surface, and the blue dashed line is the water table.

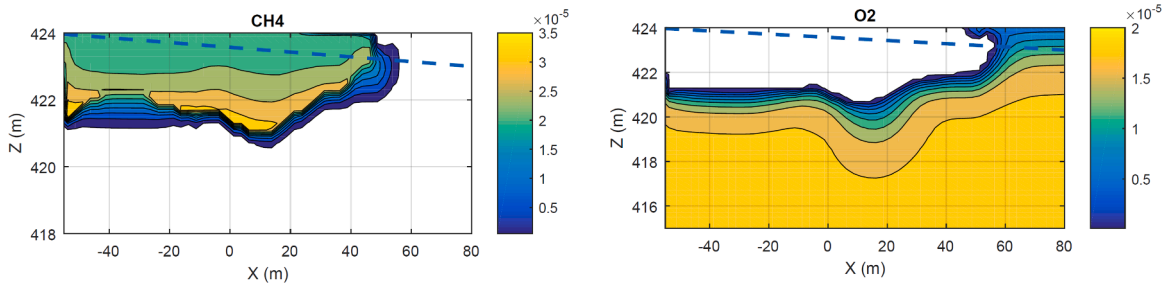

Fig. 6. Depth section of the mole fraction of methane (CH_4 – left panel) and oxygen (O_2 – right panel) in the aqueous phase after 27 years of simulation. The blue dashed line is the water table.

Table 1
Comparison between the model outputs and interpolated measurements (year 27) reported in the literature. $Z = 426$ m (2 m above the groundwater table) for the first three variables and $Z = 422$ m (2 m below the groundwater) for the last two variables.

	X (m) =	−40	−20	0	20	40	Ref.
Oxygen (g)	Measurement	<0.01	<0.01	<0.01	<0.01	<0.01	(Jones et al., 2014; Molins et al., 2010)
Mole frac.	Model	0.005	0.004	0.001	0.001	0.009	–
CO_2 (g)	Measurement	0.1	0.15	0.10	0.15	0.10	(Jones et al., 2014; Molins et al., 2010)
Mol frac.	Model	0.12	0.14	0.16	0.16	0.11	-
CH_4 (g)	Measurement	0.05	0.05	0.10	0.10	0.05	(Jones et al., 2014; Molins et al., 2010)
Mole frac.	Model	0.05	0.08	0.14	0.12	0.05	–
Temperature increase (°C)	Measurement	1.5	2	3	2.5	2.2	(Warren and Bekins, 2015)
	Model	1.8	2.3	2.8	2.4	1.9	-
DO mM	Measurement	<0.1	<0.1	<0.1	<0.1	<0.1	(Ng et al., 2014)
	Model	0.003	0.001	0.001	0.002	0.005	–

of NVDOCs. We also consider a constant rate of preNVDOC to NVDOC conversion (Ng et al., 2015). The description, stoichiometry and reaction constants are summarised in the Appendix (Tables A1 and A2) (Essaid et al., 1995; Molins et al., 2010).

The non-competitive inhibitors include oxygen for Fe(III) and Mn (IV) reduction and methanogenesis, Mn(IV) for Fe(III) reduction and toluene and short and long chain alkanes for the conversion of pre-NVDOC to NVDOC (Essaid et al., 1995; Ng et al., 2015). The heat generation rate for aerobic degradation of methane is reported to be 865 kJ/mol (Warren and Bekins, 2015).

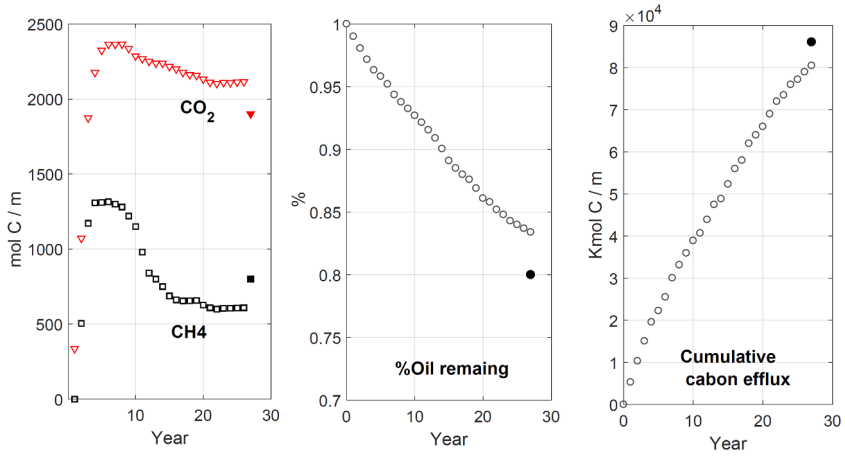

Fig. 7. Temporal variation of modeling results (non-filled markers) of the methane and carbon dioxide (both in the gaseous phase - moles carbon per one metre width) (left), the percentage of the remaining LNAPL mass (middle) and the carbon loss (in kilomoles carbon per metre width) (right). Field measurements (year 27 - filled markers) are from (Jones et al., 2014; Ng et al., 2014).

Table A1
Index of the components and reactions applied in the model.

Index	Components	Reaction	Index	Components	Reaction
1	Water	Aerobic degradation- BEX	11	Residual	Mn reduction- Short alkanes
2	N_2	Fe reduction- BEX	12	Fe III	Methanogenesis- Short alkanes
3	O_2	Mn reduction-BEX	13	Mn IV	Aerobic degradation- Long alkanes
4	CO_2	Methanogenesis-BEX	14	Fe II	Mn reduction- Long alkanes
5	CH_4	Aerobic degradation- Tol.	15	Mn II	Aerobic degradation- Methane
6	BEX	Fe reduction- Tol.	16	NVDOC	Methanogenesis- Long alkanes.
7	Toluene	Mn reduction-Tol	17	–	Aerobic degradation- NVDOC
8	Short alk.	Methanogenesis-Tol.	18	–	Fe reduction- NVDOC.
9	Long alk.	Aerobic degradation- Short alkanes.	19	–	Methanogenesis- NVDOC.
10	preNVDOC	Fe reduction- Short alkanes.	20		PreNVDOC=> NVDOC

Total number of grid cells is 15,600. The simulation time is 27 years (~10,000 days), consistent with the majority of the studies for the Bemidji site. The boundary conditions are of Dirichlet type. TMVOCBio was activated on the CSIRO Pearcey cluster, which is a 20-core / node machine. We used 15 nodes and the total wall time was around 300 h. All the input and output files (MESH, INCON, INFILE, SAVE, GENER) are provided as Supplementary Material.

5. Results and discussion

5.1. Description and intercomparison

Results are presented for microbial population distributions (Fig. 3), soil gas concentration changes (Fig. 4), temperature and LNAPL saturations (Fig. 5) and dissolved concentration changes (Fig. 6). Largely, predictions are shown at the end of the simulation – after 27 years where field data are available for comparison.

Fig. 3 shows depth section profiles of aerobic and methanogenic microbial colonies after 7 and 27 years of NSZD. The aerobic microbes mostly reside in the upper part of the vadose zone, shaped like a dome covering the LNAPL saturation distribution. This reflects the abundance of oxygen at shallower depths, but also reflects the zone where microbes oxidise methane gas that migrates to shallower depths of the soil profile.

The methanogenic microbial colony increased its biomass over time. It's distribution largely coincides with the LNAPL saturation zone, where methane is produced. It is also where the soil permeability to the gas phase and abundance of oxygen is lower. The methanogens grow first in the vicinity of the groundwater table and expands upwards through the vadose zone as time proceeds. Evolution of the microbial colonies over time is visualised in video clip #1 in the Supplementary Materials.

Fig. 4 shows the depth section profiles of oxygen, methane, carbon dioxide and BEX in the gaseous phase. Oxygen concentrations are depleted in the vicinity of the LNAPL. The maximum lateral extent of the oxygen depletion near the depth of the water table is about $X = 70$ m; beyond this distance atmospheric oxygen penetrates nearly to the depth of the water table. Methane concentrations in the gas phase largely envelope the LNAPL saturation distribution in and above the capillary fringe. This also coincides with the maximum methanogenic microbial colony biomass and where oxygen is less abundant.

The pattern and magnitude of the oxygen and methane gas concentrations are consistent with reported measurements in Jones et al. (2014) (Fig. 2) and Molins et al. (2010) (Fig. 3) (also see Table 1). This also aligns with the methane production zone at the site (Jones et al. (2014) (Fig. 3). Evolution of these gas-phase profiles over time is visualised in video clip #2 in the Supplementary Materials. The video clip also includes the simulated evolution of BEX, carbon dioxide, methane, toluene and short-chain alkanes in the gaseous phase over time. Together, Figs. 3 and 4 depict the balance of methane production and degradation and oxygen depletion.

Fig. 5 shows depth sections of the temperature and LNAPL saturation after 27 years but additionally for temperature over even deeper depths below the water table. The maximum temperature is observed around the LNAPL plume in the vadose zone extending from approximately −40 to +35 m This is the active biodegradation zone for methane production but also overlaps with the zone of methane oxidation. The temperature profile in the aqueous phase is consistent with the reported values in the literature for the Bemidji site (e.g. Fig. 6 in Warren and Bekins, 2015) (also see Table 1). The LNAPL saturation (SN) plume near the water table expands slightly downgradient (compared to the initial distribution in Fig. 2) due to groundwater flow but the change is marginal. This is also where the LNAPL saturation is higher and hence the relative permeability of the LNAPL phase is greater. Video clip #1 in the

Table A2

Stoichiometry of the biochemical reactions. Column 1is the reaction index (see Table A1), *S* (column 2) represents the primary substrate index (Table A1), *React.* represents the type of reaction (*A*: aerobic, *Fe*: Fe reduction, *Mn*: Mn reduction and *Met*: methanogenesis), columns 4–19 represent the moles of the substrate indexed in the column header (negative values show production and positive values show consumption), μ_m ($\times 10^{-6}$) is the maximum specific substrate degradation rate, $K_{s1,2}$ ($\times 10^{-6}$) represent the half saturation of the primary and secondary substrates, nC_{1-3} represent the non-competitive inhibitor index (Table A1) and K_{nC1-3} represent the non-competitive inhabitation coefficients. Please refer to the code manual (Battistelli, 2004) and the provided files (SAVE and INFILE) for further information.

	S	*Reac.*	*1*	*2*	*3*	*4*	*5*	*6*	*7*	*8*	*9*	*10*	*11*	*12*	*13*	*14*	*15*	*16*	K_S	K_E	nC_1	nC_2	nC_3	K_{nC1}	K_{Nc2}	K_{nC3}
#1	6	A	−3	0	7.5	−6	0	1	0	0	0	0	0	0	0	0	0	0	1	1						
#2	6	Fe	−24	0	0	−6	0	1	0	0	0	0	0	30	0	−30	0	0	1	50	3	13		0.8	0.01	
#3	6	Mn	0	0	0	−6	0	1	0	0	0	0	0	0	15	0	−15	0	1	15	3			0.8		
#4	6	Met	18	0	0	−9	15	1	0	0	0	0	0	0	0	0	0	0	0.12	–	3			1.6		
#5	7	A	−4	0	9	−7	0	0	1	0	0	0	0	0	0	0	0	0	1	1						
#6	7	Fe	−28	0	0	−7	0	0	1	0	0	0	0	36	0	−36	0	0	1	50	3	13		0.8	0.01	
#7	7	Mn	0	0	0	−7	0	0	1	0	0	0	0	0	18	0	−18	0	1	15	3			0.8		
#8	7	Met	10	0	0	−5	−9	0	2	0	0	0	0	0	0	0	0	0	0.12	–	3			1.6		
#9	8	A	−50	0	69	−44	0	0	0	4	0	0	0	0	0	0	0	0	1	1						
#10	8	Fe	−55	0	0	−11	0	0	0	1	0	0	0	69	0	−69	0	0	1	20	3	13		0.8	0.01	
#11	8	Mn	0	0	0	−22	0	0	0	2	0	0	0	0	69	0	−69	0	1	15	3			0.8		
#12	8	Met	38	0	0	−19	−69	0	0	8	0	0	0	0	0	0	0	0	0.12	–	3			1.6		
#13	9	A	−16	0	23	−15	0	0	0	0	1	0	0	0	0	0	0	0	1	1						
#14	9	Mn	0	0	0	−15	0	0	0	0	1	0	0	0	−46	0	0	0	1	15	3			0.8		
#15	5	A	−1	0	2	−1	1	0	0	0	0	0	0	0	0	0	0	0	2	2				0.8		
#16	9	Met	14	0	0	−7	−23	0	0	0	2	0	0	0	0	0	0	0	0.12	–	3			1.6		
#17	16	A	−12	0	22	−19	0	0	0	0	0	0	0	0	0	0	0	1	1	1						
#18	16	Fe	−57	0	0	−19	0	0	0	0	0	0	0	88	0	−88	0	1	1	50	3	13		0.8	0.01	
#19	16	Met	10	0	0	−8	−11	0	0	0	0	0	0	0	0	0	0	1	1	0.12	3			1.2		
#20	10	–	0	0	0	0	0	0	0	0	0	1	0	0	0	0	0	−1	1E6	–	7	8	9	30	30	30

Supplementary Materials visualises the evolution of the temperature and LNAPL profile over the 27 year period.

Fig. 6 shows methane and oxygen concentration depth section distributions in the aqueous phase. For methane, the aqueous phase concentration is observed in the soil moisture of the vadose zone (due to equilibrium with the gas phase) and the groundwater in the saturated zone. The vertical and horizontal extent of the methane and oxygen profile in the saturated zone is consistent with the measurements reports for Bemidji (Fig. SI2 (measurements)) by Ng et al. (2015). Note that the horizontal groundwater flow at the LNAPL zone deviates towards the depth due to the preferential flow direction in higher relative permeability direction. Also, the growth of methanogen microbial colonies at depth causes methane formation. The lateral and vertical extent of the oxygen depletion region in the aqueous phase is generally consistent with the measurements in the literature. The measurements and modeling results in (Ng et al., 2014) (Fig. 5) and (Ng et al., 2015) (Figs. 2, SI2 and SI3) show that the aqueous oxygen-depleted and aqueous methane plume in year 27 reach 418 m and 80 m in Z and X directions respectively. However, the results here show slightly smaller plumes in the aqueous phase, although the overall plume architecture is replicated. This is potentially due to the assumption we made on the intrinsic permeability in X direction, which may be improved in a calibration trial.

In the vadose zone, the oxygen depletion zone in the gaseous and aqueous phases are consistent. Video clip #3 in the Supplementary Materials visualises the evolution of methane and oxygen concentrations in the aqueous phase over time. The video clip also shows aqueous phase concentration transitions for BEX and short chain alkanes.

Fig. 7 shows the temporal variation of modeling results (non-filled markers) vs. the final measurements (filled markers Jones et al. 2014, Ng et al. 2014) of methane and carbon dioxide (both in the gaseous phase) in moles carbon per metre width, the percentage of the remaining LNAPL and the carbon loss in kilomoles carbon per metre width. Overall, despite a lack of model calibration and parameter adjustment, an acceptable consistency is observed between the field measurements and the modeling results. This is additional to good comparisons indicated earlier for depth section gas, aqueous and other field measurements.

5.2. *Brief discussion*

As shown by the agreement of model estimates and site measurements, the underlying processes governing NSZD at the Bemidji site seem to be reasonably well represented by the digital twin computational modeling platform. Of course, some elements of the model are difficult to validate such as microbial community populations/biomass for each individual community. Often consortia of microbes are involved in biodegradation processes, not just a few groups (Bruckberger et al., 2021). Regardless, as indicated in several figures (e.g., Figs. 5–7), predicted model estimates for temperature and gaseous concentrations as well as integrated properties (remaining oil and cumulative carbon dioxide efflux) are in close correspondence to the site measurements. For such a case it could be argued that the underlying assumptions about microbial communities and the rates at which they operate are reasonable (albeit bulked) approximations within the model structure.

The success of the modeling strategy in developing a digital twin for a complex LNAPL-impacted subsurface system relies on the representativeness of the conceptual model and the governing equations. This needs to link to adequately comprehensive data and information. For subsurface systems such as the one here, phenomena are studied at a Darcy scale. This enjoins that the fundamental governing equations (such as the (Navier-)Stokes equation for the flow field) are upscaled (Xiong et al., 2016; Yan et al., 2017). Consequently, parameters become averaged or are lumped. A good example is the pore scale architecture translated (through empirical constitutive relationships) to bulk coefficients such as tortuosity and permeability (Tartakovsky et al., 2013).

Such scaling seems to have been well enough represented via processes and parameter values used in the model simulations.

Some of the assumptions resulting in Darcy scale modeling of multi-phase systems have been extensively studied. For instance, it is believed that the equilibrium partitioning assumption holds (Lekmine et al., 2017). However, subsurface modeling at a Darcy scale still has some limitations with respect to the constitutive relationships. For instance, it is not very clear how changes in the LNAPL composition would change the hysteresis and capillary effects over the time (Sookhak Lari et al., 2016a). This has not been included in the simulations here, but may be important in certain circumstances – such as where water tables or soil moisture might be dynamic.

Furthermore, biochemical processes like chemotaxis, changes of the geophysical properties due to e.g., changes in the biofilms thickness and the food-chain are not yet thoroughly quantified at a Darcy scale (Bahar et al., 2016; Essaid et al., 2015; Tartakovsky et al., 2013; Wang et al., 2016). These parameters are still mostly lumped into e.g., yield and decay coefficients of the microbial colonies. Even for a comprehensively studied site like Bemidji, some discrepancies may be observed in the ranges of the biochemical parameters (Essaid et al., 2011). A possible reason is that these lumped parameters are non-linearly interconnected and (from a mathematical point of view) it is possible to have ranges for the parameters, while the overall modeling output remains reasonable. However, a universal approach across sites, either requires a modeling concept with the least number of lumped parameters or comprehensive site characterization to determine such parameters.

Regardless, as indicated earlier, the implication for the Bemidji site is that the key acceptable processes (NAPL, air, water mobility; partitioning; biodegradation in soil and groundwater) when linked together in the digital twin platform with parameter values in reasonable ranges have reproduced field-measured components (such as NAPL components, oxygen and evolved gases) with required reliability. Through the approach discussed here and the supplementary information supplied, it is possible to simulate and predict NSZD processes over long periods, for example over decades. It is technically possible to investigate the trade-off between active multi-phase remediation approaches and NSZD to enhance the LNAPL mass recovery and minimise costs, energy consumption and the broader carbon footprint of management at petroleum impacted sites. The digital twin platform for this (and any similar) site enables optimizing management plans (Sookhak Lari et al., 2019b). For instance, it may be that selective targeting of LNAPL components through active remediation, yields higher overall NSZD mass removal over time. The fully-developed digital twin would be a reliable, efficient and non-invasive affordable approach for better assessment of such management options.

6. Conclusion

The long-term reliability of NSZD as a management option is yet to be fully established. Predictive capability is needed that links all fundamental fluid dynamic aspects of LNAPL/air/water relative mobility together with all aspects of partitioning and biodegradation of LNAPL components in water, air and soil phases of subsurface systems. This has been shown to be possible utilising TMVOCBio in creating a simulation platform and progressing a digital twin of NSZD processes. This has required accommodating all fundamental processes from the ground surface, through the vadose zone and into deeper groundwater – a scope not undertaken previously.

Advances in computational infrastructure plus the recently released parallel-processing version of the TMVOCBio has allowed feasible and affordable simulation to progress the idea of developing a digital twin for such complex subsurface processes. The capability is also applicable to addressing greenhouse gas emissions through anthropogenic sources of soil contamination, which has been accounted for as a considerable driver of global warming (King and Durham, 2017).

We evaluated (and in part verified) the multi-phase multi-component multi-microbe and non-isothermal modeling framework by simulating the well characterised oil-contaminated Bemidji site. With little calibration, the digital twin simulation platform matched Bemidji field data for soil gas and aqueous phase concentrations, temperature and overall LNAPL and carbon dioxide mass estimates. The approach is computationally affordable, applicable and feasible for NSZD. It provides a platform to estimate the longevity and changes to NSZD rates over decades to centuries, and a platform that offers the potential to co-simulate NSZD and other remedial option scenarios concurrently. The latter promises to assist decision making regarding residual risk from LNAPL and in deciding when to cease active remedial activities compared to ongoing management of LNAPL mass and risk using an NSZD approach.

Future work is still needed to develop a solid basis for real digital twins for complex systems such as the one studied here. This is mainly needed in two fields: 1- advancing the underlying physics and governing equation to include processes such as chemotaxis, food chain, bubble formation and mutations in the microbial colonies and 2- more comprehensive constitutive relationships for multiphase systems (Sookhak Lari et al., 2019a). Furthermore, the core model applied here does not have the capabilities to include biochemical kinetic reactions, such as those in TOUGHREACT (Xu et al., 2004).

Due to its complex and multi-disciplinary nature, advancing the digital tools to study subsurface system requires significant motivation and resourcing. Here, it is noted that about one-third of global methane released is by methanogenesis from soils, (Bossio et al., 2020). A considerable portion of this is anthropogenic, such as LNAPL release incidents. A study on global distributed oil-contaminated lands may provide momentum to accelerate and motivate advances in capability. The study presented contributes to this.

Declaration of Competing Interest

The authors declare that they have no known competing financial interests or personal relationships that could have appeared to influence the work reported in this paper.

Supplementary materials

Supplementary material associated with this article can be found, in the online version, at doi:10.1016/j.watres.2021.117853.

Appendix

Tables A1 and A2

References

Amos, R.T., Mayer, K.U., 2006. Investigating the role of gas bubble formation and entrapment in contaminated aquifers: reactive transport modeling. J. Contam. Hydrol. 87 (1), 123–154.

Baedecker, M.J., Cozzarelli, I.M., Eganhouse, R.P., Siegel, D.I., Bennett, P.C., 1993. Crude oil in a shallow sand and gravel aquifer—III. Biogeochemical reactions and mass balance modeling in anoxic groundwater. Appl. Geochem. 8 (6), 569–586.

Baedecker, M.J., Eganhouse, R.P., Qi, H., Cozzarelli, I.M., Trost, J.J., Bekins, B.A., 2018. Weathering of oil in a surficial aquifer. Groundwater 56 (5), 797–809.

Bahar, T., Golfier, F., Oltéan, C., Benioug, M., 2016. An upscaled model for bio-enhanced NAPL dissolution in porous media. Transp. Porous Media 113 (3), 653–693.

Barry, D.A., Prommer, H., Miller, C.T., Engesgaard, P., Brun, A., Zheng, C., 2002. Modeling the fate of oxidisable organic contaminants in groundwater. Adv. Water Resour. 25 (8), 945–983.

Battistelli, A., 2004. Modeling biodegradation of organic contaminants under multiphase conditions with TMVOCBio. Vadose Zone J. 3, 875–883.

Bekins, B.A., Cozzarelli, I.M., Godsy, E.M., Warren, E., Essaid, H.I., Tuccillo, M.E., 2001. Progression of natural attenuation processes at a crude oil spill site: II. Controls on spatial distribution of microbial populations. J. Contam. Hydrol. 53 (3), 387–406.

Bekins, B.A., Hostettler, F.D., Herkelrath, W.N., Delin, G.N., Warren, E., Essaid, H.I., 2005. Progression of methanogenic degradation of crude oil in the subsurface. Environ. Geosci. 12 (2), 139–152.

Blanc, P.C.D., McKinney, D.C., Speitel, G.E., Corapcioglu, M.Y., 1996. Advances in Porous Media. Corapcioglu. Elsevier, pp. 1–86.

Boschert, S., Rosen, R., Hehenberger, P., Bradley, D., 2016. Mechatronic Futures: Challenges and Solutions for Mechatronic Systems and Their Designers. Springer International Publishing, Cham, pp. 59–74.
Bossio, D.A., Cook-Patton, S.C., Ellis, P.W., Fargione, J., Sanderman, J., Smith, P., Wood, S., Zomer, R.J., von Unger, M., Emmer, I.M., Griscom, B.W., 2020. The role of soil carbon in natural climate solutions. Nat. Sustain. 3 (5), 391–398.
Bruckberger, M.C., Gleeson, D.B., Bastow, T.P., Morgan, M.J., Walsh, T., Rayner, J.L., Davis, G.B., Puzon, G.J., 2021. Unravelling microbial communities associated with different light non-aqueous phase liquid types undergoing natural source zone depletion processes at a legacy petroleum site. Water 13 (7) (Basel).
Chang, J.I., Lin, C.C., 2006. A study of storage tank accidents. J. Loss Prev. Process. Ind. 19 (1), 51–59.
Chilvers, B.L., Morgan, K.J., White, B.J., 2021. Sources and reporting of oil spills and impacts on wildlife 1970–2018. Environ. Sci. Pollut. Res. 28 (1), 754–762.
Conejos Fuertes, P., Martínez Alzamora, F., Hervás Carot, M., Alonso Campos, J.C., 2020. Building and exploiting a digital twin for the management of drinking water distribution networks. Urban Water J. 17 (8), 704–713.
Cozzarelli, I.M., Bekins, B.A., Baedecker, M.J., Aiken, G.R., Eganhouse, R.P., Tuccillo, M. E., 2001. Progression of natural attenuation processes at a crude-oil spill site: I. Geochemical evolution of the plume. J. Contam. Hydrol. 53 (3), 369–385.
CRC-CARE, 2018. CRC CARE Technical Report No. 44. CRC for Contamination Assessment and Remediation of the Environment, Newcastle, Australia.
Davis B, G, Knight H, J, Rayner L, J, 2021. Extinguishing petroleum vapor intrusion and methane risks for slab-on-ground buildings: a simple guide. Groundwater Monitoring and Remediation 41 (2), 61–72. https://doi.org/10.1111/gwmr.12440.
Davis, G.B., Laslett, D., Patterson, B.M., Johnston, C.D., 2013. Integrating spatial and temporal oxygen data to improve the quantification of *in situ* petroleum biodegradation rates. J. Environ. Manag. 117, 42–49.
Dillard, L.A., Essaid, H.I., Herkelrath, W.N., 1997. Multiphase flow modeling of a crude-oil spill site with a bimodal permeability distribution. Water Resour. Res. 33 (7), 1617–1632.
Essaid, H.I., Bekins, B.A., Cozzarelli, I.M., 2015. Organic contaminant transport and fate in the subsurface: evolution of knowledge and understanding. Water Resour. Res. 51 (7), 4861–4902.
Essaid, H.I., Bekins, B.A., Godsy, E.M., Warren, E., Baedecker, M.J., Cozzarelli, I.M., 1995. Simulation of aerobic and anaerobic biodegradation processes at a crude oil spill site. Water Resour. Res. 31 (12), 3309–3327.
Essaid, H.I., Bekins, B.A., Herkelrath, W.N., Delin, G.N., 2011. Crude oil at the bemidji site: 25 years of monitoring, modeling, and understanding. Gr. Water 49 (5), 706–726.
Essaid, H.I., Cozzarelli, I.M., Eganhouse, R.P., Herkelrath, W.N., Bekins, B.A., Delin, G.N., 2003. Inverse modeling of BTEX dissolution and biodegradation at the Bemidji, MN crude-oil spill site. J. Contam. Hydrol. 67 (1), 269–299.
Etkin, D.E., 2009a. Analysis of U.S. Oil Spillage. API, USA.
Etkin, D.S., 2001. Analysis of oil spill trends in the united states and worldwide. Int. Oil Spill Conf. Proc. 2001 (2), 1291–1300.
Etkin, D.S., 2009b. 40-year Analysis of US Oil Spillage Rates. Environment Canada, Canada, p. 1332.
Fingas, M., 2012. The Basics of Oil Spill Cleanup. CRC Press, pp. 22–39.
Freitas, J.G., Doulatyari, B., Molson, J.W., Barker, J.F., 2011a. Oxygenated gasoline release in the unsaturated zone, part 2: downgradient transport of ethanol and hydrocarbons. J. Contam. Hydrol. 125 (1), 70–85.
Freitas, J.G., Mocanu, M.T., Zoby, J.L.G., Molson, J.W., Barker, J.F., 2011b. Migration and fate of ethanol-enhanced gasoline in groundwater: a modeling analysis of a field experiment. J. Contam. Hydrol. 119 (1), 25–43.
Garg, S., Newell, C.J., Kulkarni, P.R., King, D.C., Adamson, D.T., Renno, M.I., Sale, T., 2017. Overview of natural source zone depletion: processes, controlling factors, and composition change. Groundw. Monit. Remediat. 37 (3), 62–81.
Grieves, M., Vickers, J., Kahlen, F.J., Flumerfelt, S., Alves, A., 2017. Transdisciplinary Perspectives on Complex Systems: New Findings and Approaches. Springer International Publishing, Cham, pp. 85–113.
Jones, K.L., Lindsay, M.B.J., Kipfer, R., Mayer, K.U., 2014. Atmospheric noble gases as tracers of biogenic gas dynamics in a shallow unconfined aquifer. Geochim. Cosmochim. Acta 128, 144–157.
Jung, Y., Battistelli, A., 2017. User's guide for biodegradation reactions in TMVOCBio LBNL-1005179. Lawrence Berkeley National Laboratory, California. United States.
Jung, Y., Pau, G.S.H., Finsterle, S., Pollyea, R.M., 2017. TOUGH3: a new efficient version of the TOUGH suite of multiphase flow and transport simulators. Comput. Geosci. 108, 2–7.
Karimi Askarani, K., Sale, T.C., 2020. Thermal estimation of natural source zone depletion rates without background correction. Water Res. 169, 115245.
Khan, F.I., Abbasi, S.A., 1999. Major accidents in process industries and an analysis of causes and consequences. J. Loss Prev. Process Ind. 12 (5), 361–378.
King, G.E., Durham, D., Schug, K.A., Hildenbrand, Z.L., 2017. Advances in Chemical Pollution, Environmental Management and Protection. Elsevier, pp. 257–274.
Knight, J.H., Davis, G.B., 2013. A conservative vapour intrusion screening model of oxygen-limited hydrocarbon vapour biodegradation accounting for building footprint size. J. Contam. Hydrol. 155, 46–54.
Krol, M.M., Mumford, K.G., Johnson, R.L., Sleep, B.E., 2011. Modeling discrete gas bubble formation and mobilization during subsurface heating of contaminated zones. Adv. Water Resour. 34 (4), 537–549.
Kulkarni, P.R., Newell, C.J., King, D.C., Molofsky, L.J., Garg, S., 2020. Application of four measurement techniques to understand natural source zone depletion processes at an LNAPL site. Groundw. Monit. Remediat. 40 (3), 75–88.
Lekmine, G., Sookhak Lari, K., Johnston, C.D., Bastow, T.P., Rayner, J.L., Davis, G.B., 2017. Evaluating the reliability of equilibrium dissolution assumption from residual gasoline in contact with water saturated sands. J. Contam. Hydrol. 196, 30–42.
Lenhard, R.J., Parker, J.C., 1990. Estimation of free hydrocarbon volume from fluid levels in monitoring wells. Groundwater 28 (1), 57–67.
Lenhard, R.J., Sookhak Lari, K., Rayner, J.L., Davis, G.B., 2018. Evaluating an analytical model to predict subsurface LNAPL distributions and transmissivity from current and historic fluid levels in groundwater wells: comparing results to numerical simulations. Groundw. Monit. Remediat. 38 (1), 75–84.
Liu, M., Fang, S., Dong, H., Xu, C., 2021. Review of digital twin about concepts, technologies, and industrial applications. J. Manuf. Syst. 58, 346–361.
Mayer, K.U., Frind, E.O., Blowes, D.W., 2002. Multicomponent reactive transport modeling in variably saturated porous media using a generalized formulation for kinetically controlled reactions. Water Resour. Res. 38 (9), 13-11–13-21-13.
Miller, C.T., Dawson, C.N., Farthing, M.W., Hou, T.Y., Huang, J., Kees, C.E., Kelley, C.T., Langtangen, H.P., 2013. Numerical simulation of water resources problems: models, methods, and trends. Adv. Water Resour. 51, 405–437.
Molins, S., Mayer, K.U., Amos, R.T., Bekins, B.A., 2010. Vadose zone attenuation of organic compounds at a crude oil spill site — interactions between biogeochemical reactions and multicomponent gas transport. J. Contam. Hydrol. 112 (1), 15–29.
Molson, J.W., Barker, J.F., Frind, E.O., Schirmer, M., 2002a. Modeling the impact of ethanol on the persistence of benzene in gasoline-contaminated groundwater. Water Resour. Res. 38 (1), 4-1–4-12-14.
Molson, J.W., Frind, E.O., Stempvoort, D.R.V., Lesage, S., 2002b. Humic acid enhanced remediation of an emplaced diesel source in groundwater: 2. Numerical model development and application. J. Contam. Hydrol. 54 (3), 277–305.
Ng, G.-H.C., Bekins, B.A., Cozzarelli, I.M., Baedecker, M.J., Bennett, P.C., Amos, R.T., Herkelrath, W.N., 2015. Reactive transport modeling of geochemical controls on secondary water quality impacts at a crude oil spill site near Bemidji, MN. Water Resour. Res. 51 (6), 4156–4183.
Ng, G.H.C., Bekins, B.A., Cozzarelli, I.M., Baedecker, M.J., Bennett, P.C., Amos, R.T., 2014. A mass balance approach to investigating geochemical controls on secondary water quality impacts at a crude oil spill site near Bemidji, MN. J. Contam. Hydrol. 164, 1–15.
Parker, J.C., Lenhard, R.J., 1987. A model for hysteretic constitutive relations governing multiphase flow: 1. Saturation-pressure relations. Water Resour. Res. 23 (12), 2187–2196.
Pruess, K., Battistelli, A., 2002. TMVOC, A Numerical Simulator for Three-Phase Non-Isothermal Flows of Multicomponent Hydrocarbon Mixtures in Saturated-Unsaturated Heterogeneous Media. Lawrence Berkeley National Laboratory, Berkeley, USA.
Rayner, J.L., Bekele, E., Donn, M., Bastow, T., Davis, G.B., Woodbury, R., Furness, A., Geste, Y., 2020. Australian Case Studies of Light Non-Aqueous Phase Liquid (LNAPL) natural Source Zone Depletion Rates Compared with Conventional Active Recovery Efforts. CRC CARE Technical Report.
Sihota, N.J., Singurindy, O., Mayer, K.U., 2011. CO2-efflux measurements for evaluating source zone natural attenuation rates in a petroleum hydrocarbon contaminated aquifer. Environ. Sci. Technol. 45 (2), 482–488.
Smith, J.J., Benede, E., Beuthe, B., Marti, M., Lopez, A.S., Koons, B.W., Kirkman, A.J., Barreales, L.A., Grosjean, T., Hjort, M., 2021. A comparison of three methods to assess natural source zone depletion at paved fuel retail sites. Q. J. Eng. Geol. Hydrogeol. 54 (4) qjegh2021 qjegh2005.
Sookhak Lari, K., Davis, G.B., Johnston, C.D., 2016a. Incorporating hysteresis in a multi-phase multi-component NAPL modeling framework; a multi-component LNAPL gasoline example. Adv. Water Resour. 96, 190–201.
Sookhak Lari, K., Davis, G.B., Rayner, J.L., Bastow, T.P., Puzon, G.J., 2019a. Natural source zone depletion of LNAPL: a critical review supporting modeling approaches. Water Res. 157, 630–646.
Sookhak Lari, K., Johnston, C.D., Davis, G.B., 2015. Interfacial mass transport in porous media augmented with bulk reactions: analytical and numerical solutions. Transp. Porous Media 106 (2), 405–423.
Sookhak Lari, K., Johnston, C.D., Davis, G.B., 2016b. Gasoline multiphase and multicomponent partitioning in the vadose zone: dynamics and risk longevity. Vadose Zone J. 15 (3).
Sookhak Lari, K., Johnston, C.D., Rayner, J.L., Davis, G.B., 2018a. Field-scale multi-phase LNAPL remediation: validating a new computational framework against sequential field pilot trials. J. Hazard. Mater. 345, 87–96.
Sookhak Lari, K., King, A., Rayner, J.L., Davis, G.B., 2021. Quantifying the benefits of in-time and in-place responses to remediate acute LNAPL release incidents. J. Environ. Manag. 287, 112356.
Sookhak Lari, K., Rayner, J.L., Davis, G.B., 2017. A computational assessment of representative sampling of soil gas using existing groundwater monitoring wells screened across the water table. J. Hazard. Mater. 335, 197–207.
Sookhak Lari, K., Rayner, J.L., Davis, G.B., 2018b. Towards characterizing LNAPL remediation endpoints. J. Environ. Manag. 224, 97–105.
Sookhak Lari, K., Rayner, J.L., Davis, G.B., 2019b. Toward optimizing LNAPL remediation. Water Resour. Res. 55 (2), 923–936.
Sookhak Lari, K., Rayner, J.L., Davis, G.B., Johnston, C.D., 2020. LNAPL recovery endpoints: lessons learnt through modeling, experiments, and field trials. Groundw. Monit. Remediat. 40, 21–29. https://doi.org/10.1111/gwmr.12400.
Tartakovsky, G.D., Tartakovsky, A.M., Scheibe, T.D., Fang, Y., Mahadevan, R., Lovley, D. R., 2013. Pore-scale simulation of microbial growth using a genome-scale metabolic model: implications for darcy-scale reactive transport. Adv. Water Resour. 59, 256–270.
VanDerHorn, E., Mahadevan, S., 2021. Digital twin: generalization, characterization and implementation. Decis. Support Syst., 113524

Verginelli, I., Baciocchi, R., 2021. Refinement of the gradient method for the estimation of natural source zone depletion at petroleum contaminated sites. J. Contam. Hydrol. 241, 103807.
Wang, X., Lanning, L.M., Ford, R.M., 2016. Enhanced retention of chemotactic bacteria in a pore network with residual NAPL contamination. Environ. Sci. Technol. 50 (1), 165–172.
Warren, E., Bekins, B.A., 2015. Relating subsurface temperature changes to microbial activity at a crude oil-contaminated site. J. Contam. Hydrol. 182, 183–193.
Xiong, Q., Baychev, T.G., Jivkov, A.P., 2016. Review of pore network modeling of porous media: experimental characterisations, network constructions and applications to reactive transport. J. Contam. Hydrol. 192, 101–117.
Xu, T., Sonnenthal, E., Spycher, N., Pruess, K., 2004. TOUGHREACT User's guide: A simulation Program For Non-Isothermal Multiphase Reactive Geochemical Transport in Variable Saturated Geologic Media. Lawrence Berkeley National Lab.(LBNL), Berkeley, CA (United States).
Yan, Z., Yang, X., Li, S., Hilpert, M., 2017. Two-relaxation-time lattice Boltzmann method and its application to advective-diffusive-reactive transport. Adv. Water Resour. 109, 333–342.